Article

Neuron

Amygdala Functional and Structural Connectivity Predicts Individual Risk Tolerance

Highlights

- Neural markers for risk tolerance were investigated with multimodal imaging data
- Risk tolerance correlated with amygdala-medial prefrontal cortex connectivity
- Risk tolerance correlated with amygdala structure

Authors

Wi Hoon Jung, Sangil Lee, Caryn Lerman, Joseph W. Kable

Correspondence

kable@psych.upenn.edu

In Brief

Jung et al. examine neural markers for risk tolerance in a large multimodal imaging dataset of young adults. Higher risk tolerance was associated with amygdala structure and function and with structural and functional connectivity between amygdala and medial prefrontal cortex.

Jung et al., 2018, Neuron *98*, 394–404
April 18, 2018
https://doi.org/10.1016/j.neuron.2018.03.019

CellPress

CellPress

Neuron
Article

Amygdala Functional and Structural Connectivity Predicts Individual Risk Tolerance

Wi Hoon Jung,[1] Sangil Lee,[1] Caryn Lerman,[2] and Joseph W. Kable[1,3,*]
[1]Department of Psychology, University of Pennsylvania, Philadelphia, PA 19104, USA
[2]Department of Psychiatry, Perelman School of Medicine, University of Pennsylvania, Philadelphia, PA 19104, USA
[3]Lead Contact
*Correspondence: kable@psych.upenn.edu
https://doi.org/10.1016/j.neuron.2018.03.019

SUMMARY

Risk tolerance, the degree to which an individual is willing to tolerate risk in order to achieve a greater expected return, influences a variety of financial choices and health behaviors. Here we identify intrinsic neural markers for risk tolerance in a large (n = 108) multimodal imaging dataset of healthy young adults, which includes anatomical and resting-state functional MRI and diffusion tensor imaging. Using a data-driven approach, we found that higher risk tolerance was most strongly associated with greater global functional connectivity (node strength) of and greater gray matter volume in bilateral amygdala. Further, risk tolerance was positively associated with functional connectivity between amygdala and medial prefrontal cortex and negatively associated with structural connectivity between these regions. These findings show how the intrinsic functional and structural architecture of the amygdala, and amygdala-medial prefrontal pathways, which have previously been implicated in anxiety, are linked to individual differences in risk tolerance during economic decision making.

INTRODUCTION

To make adaptive choices, decision makers must integrate their beliefs about the possible outcomes of each action with their evaluation of those possible outcomes. However, one challenge that decision makers confront is that there is often uncertainty about what outcomes will result from a given action. A particular form of uncertainty, when information about the probability of each possible outcome is known, is referred to as "risk" (von Neumann and Morgenstern, 1994). Examples of risk include the outcomes of a fair coin toss, die roll, or roulette wheel. An individual's risk tolerance (also referred to as "risk attitude" or "risk preference"), their willingness to accept risk in order to gain a greater expected return, can be measured by assessing preferences between small-but-certain and larger-but-risky rewards (Glimcher, 2008; Levy et al., 2010; Gilaie-Dotan et al., 2014). Understanding individual differences in risk tolerance is important, because risk tolerances are not only associated with financial decisions (e.g., investments, insurance) but also with smoking (Lejuez et al., 2003, 2005; Schepis et al., 2011), health behaviors (Anderson and Mellor, 2008), migration (Barsky et al., 1997; Dohmen et al., 2005), self-employment status (Ekelund et al., 2005), susceptibility to mental illness (Branas-Garza et al., 2007; Krain et al., 2008), and patients' attitude to treatment (Fraenkel et al., 2003; Barfoed et al., 2016). Here we examined neural predictors of individual differences in risk tolerance using a multimodal neuroimaging approach.

Over the past decade, functional neuroimaging studies have identified multiple brain regions engaged when making decisions involving risk (Mohr et al., 2010; Knutson and Huettel, 2015). Activity in the parietal cortex reflects the probability of outcomes (Huettel et al., 2006; Studer et al., 2015); activity in medial prefrontal cortex (mPFC) and the ventral striatum (i.e., nucleus accumbens [NAcc]) reflects an integration of the magnitude and probability of rewards for given risky options (Ernst et al., 2004; Krain et al., 2008; Levy et al., 2010); and activity in the anterior insula (aINS), anterior cingulate cortex (ACC), and amygdala reflect the degree of risk or uncertainty (Kuhnen and Knutson, 2005; Preuschoff et al., 2008; De Martino et al., 2010). Furthermore, neural activity, particularly in the NAcc, mPFC, and aINS, predicts the choice that the individual will make (Kuhnen and Knutson, 2005; Huang et al., 2014; Leong et al., 2016).

There is recent interest, though, in moving beyond predicting choice from simultaneously measured task-evoked brain activation, toward predicting behavior at greater remove, by testing whether task-independent measures of brain structure and function, from anatomical or resting-state functional MRI (RS-fMRI) or diffusion-tensor imaging (DTI), can predict decision-making tendencies (Fumagalli, 2014; Kable and Levy, 2015). For instance, increased gray matter volume (GMV) in the right posterior parietal cortex (rPPC) is associated with increased risk tolerance (Gilaie-Dotan et al., 2014; Grubb et al., 2016). Examining multiple neuroimaging modalities together, however, may provide an even better understanding of the complex interplay among brain structure and function and behavior. In a recent example, the preference for positively skewed gambles (lotteries that yield large amounts with small chances) was associated with the coherence (fractional anisotropy [FA]) of the white matter (WM) tract connecting aINS and NAcc (Leong et al., 2016), and activity in the NAcc during choice mediated the link between tract structure and choice behavior. To our knowledge, there have been no similar multimodal imaging investigations of

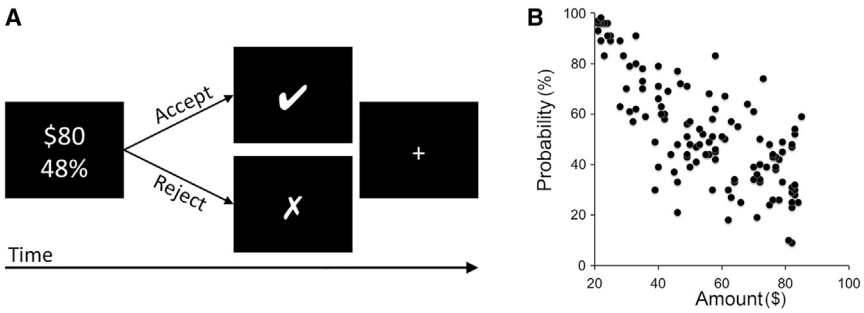

Figure 1. Risk Tolerance Task

(A) A depiction of one trial of the task. Participants chose between a smaller-certain reward (100% chance of $20) and a larger-riskier reward (e.g., 48% chance of $80) for each of 120 trials. The smaller-certain reward was fixed at 100% chance of $20 and the larger-risky reward was varied from trial to trial. Each trial began with the presentation of the risky option; the standard certain option was not shown to simplify the display. When subjects made their choice, a marker indicating that choice ("✓" if the risky option was chosen, "✗" if the certain option was chosen) appeared for 1 s. Subjects had 4 s to make their choice.

(B) Risky options used in the task. Each point represents the risky option offered on a single trial. The x axis indicates the reward amount ($) and the y axis indicates the reward probability (%).

neural markers for basic risk tolerances; identifying such markers is the goal of the present study.

We therefore examined how individual differences in risk tolerance are linked with individual variations in intrinsic functional and structural brain signatures, including resting-state functional connectivity (RSFC), GMV, and WM fiber tract strength, using multimodal, task-independent, brain imaging data in a large sample of healthy young adults (n = 108). We first identified associations between an individual's risk tolerance and different brain region's node strength, a graph-theoretical measure of the centrality of a region calculated from RS-fMRI (Rubinov and Sporns, 2010; Wang et al., 2010). This analysis highlighted the bilateral amygdalae, structures previously linked to aspects of risky decision making. To further characterize this association, we tested how RSFC to the amygdala was associated with risk tolerance using seed-based connectivity analysis, which found an association between amygdala-medial prefrontal connectivity and risk tolerance. We then identified further associations between amygdala structure (i.e., GMV) and amygdala-medial prefrontal structural connectivity (i.e., WM tract strength) and risk tolerance. Each of the identified features (structure, structural connectivity, and functional connectivity) explains unique variance in risk tolerance. This series of results identifies a coherent set of relationships between risk tolerances and multiple intrinsic functional and structural features of the amygdala and its connections with medial prefrontal cortex.

RESULTS

Risk tolerances were assessed using a well-validated task (Figure 1A; Kable et al., 2017). One hundred and eight participants (age [mean ± SD], 24.36 ± 4.69 years old; 44 females; risk tolerance α, 0.69 ± 0.31) made 120 binary choices between a certain gain of $20 and a larger-risky reward that varied from trial to trial (Figure 1B). We modeled the subjective value (SV) for each option using the functional form for expected utility. In our case, $SV = p \times A^{\alpha}$, where p and A are the reward probability and amount of winning, respectively, since there is always a $1-p$ chance of receiving nothing. α is the risk tolerance parameter; larger α values mean increased risk tolerance (see STAR Methods for a detailed explanation).

Neural Correlates of Risk Tolerance

We first tested whether risk tolerance was associated with node strength, a graph theoretic measure of the importance or centrality of a region in the resting-state functional connectivity network. Using a standard whole-brain parcellation, we calculated node strength of each parcel in the RS-fMRI dataset. The node strengths of left and right amygdalae had the highest correlation with risk tolerance (left amygdala, $r = 0.265$, $p = 0.007$; right amygdala, $r = 0.261$, $p = 0.007$; Figures 2A, 2B, and 2C). Greater amygdala node strength was associated with higher risk tolerance. Though these effects survived a false-positive adjustment used in previous studies of network measures (Lynall et al., 2010; Cocchi et al., 2012), they did not survive Bonferonni correction. Nonetheless, the fact that the strongest relationship between node strength and risk tolerance was in the amygdala led us to focus on the amygdala in subsequent analyses.

Though node strength gives an overall measure of connectivity, it does not provide anatomic specificity regarding the most important connections driving the association with risk tolerance. We next performed whole-brain seed-based (i.e., seed-to-voxel-based) connectivity analysis to further examine the relationship between amygdala RSFC and risk tolerance. There was significant positive correlation between risk tolerance and RSFC between the left amygdala and mPFC dorsally in the ACC (mPFC/ACC; peak MNI x, y, z coordinate = 3, 9, 27; peak z value = 3.68) and between risk tolerance and RSFC between the right amygdala and mPFC ventrally along the gyrus rectus (mPFC/rectus; x, y, z = −6, 9, −15; z value = 3.73; cluster-forming height threshold of $p < 0.001$, uncorrected, corrected for multiple comparisons using a cluster extent threshold of $p < 0.05$; Figure 3). The areas of mPFC identified by their connectivity to the left and right amygdala seeds overlapped at a height threshold of $p < 0.005$ (uncorrected) and cluster size correction to $p < 0.05$ for multiple comparisons across the whole brain (Figure 3). Greater amygdala-mPFC functional connectivity was associated with higher risk tolerance.

Next, based on our RSFC results described above, we examined whether risk tolerance was also associated with structural connectivity between the amygdala and mPFC. We defined mPFC targets from the above seed-based RSFC results and performed probabilistic tractography using diffusion imaging data

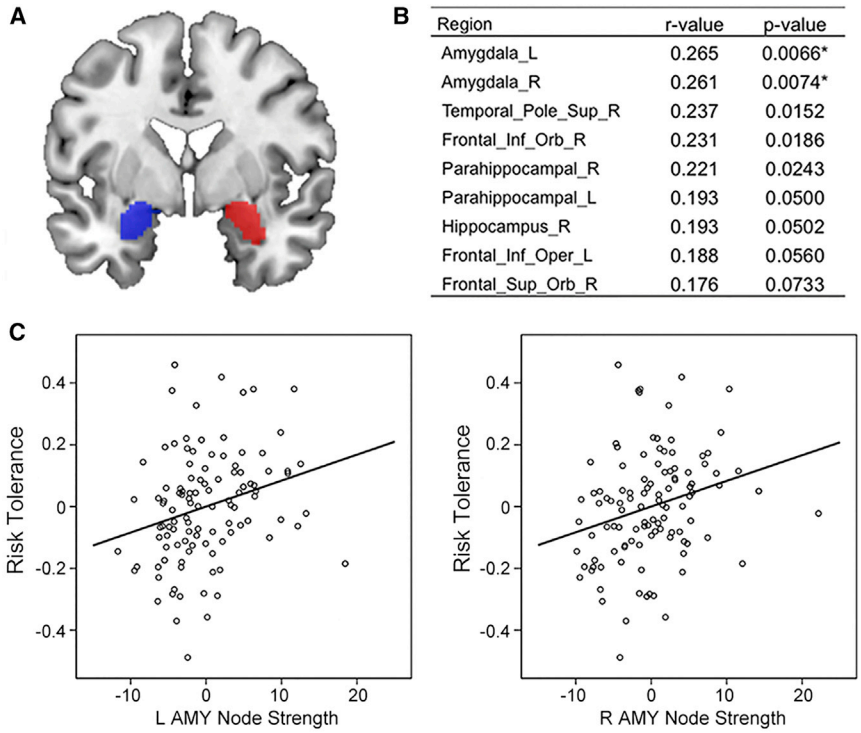

Figure 2. Significant Correlations between Risk Tolerance and Node Strengths of Resting-State Network

(A) Amygdala seeds (blue for left hemisphere; red for right hemisphere) identified by AAL template.

(B) Brain regions with the highest correlation coefficients (top 10%) between risk tolerance and node strength, calculated using graph theoretical analysis of resting-state fMRI.

(C) Partial correlation scatterplot between risk tolerance and left (right) amygdala node strength. For illustration purposes, this scatterplot was generated by performing Pearson correlation analysis between residuals after regressing out age, sex, IQ, and mean framewise displacement (motion) in the resting state scan. L, left; R, right; Sup, superior; Inf, inferior; Orb, orbito; Oper, opercular; AMY, amygdala.

(Figure 4A). The tracts between the amygdala and the mPFC coursed medially through ventral striatal regions, consistent with findings from previous probabilistic tractography studies (Croxson et al., 2005; Kim and Whalen, 2009; Clewett et al., 2014; see Figure 4B for a single subject map identified using deterministic tractography for illustration purposes only). The tract strength between right amygdala and mPFC/rectus was significantly negatively correlated with risk tolerance ($r = -0.279$, $p = 0.004$; Figure 4C). The tract strength between left amygdala and mPFC/ACC was also negatively correlated with risk tolerance ($r = -0.140$, $p = 0.155$; Figure 4D), though this relationship was not significant. Thus, greater right amygdala-mPFC tract strength was associated with lower risk tolerance.

There was an inverse relationship between WM tract strength and RSFC. The tract strength between right amygdala and mPFC/rectus exhibited a non-significant negative correlation with RSFC strength between these two regions ($r = -0.177$, $p = 0.070$), while the tract strength between left amygdala and mPFC/ACC exhibited a significant negative correlation with RSFC strength between these two regions ($r = -0.292$, $p = 0.002$).

We confirmed that the laterality of the structural connectivity effect was not due to using different target ROIs for each hemisphere. The reconstructed WM tract between amygdala and frontal cortex is particularly strong to the ventral part of mPFC (i.e., medial orbitofrontal cortex [OFC]), and the target ROI (mPFC/rectus) defined by RSFC for right amygdala is more ventrally located than that (mPFC/ACC) for left amygdala. To address this issue, we conducted additional analyses using symmetric anatomical ROIs for ventral mPFC, defined according to Automated Anatomical Labeling (AAL) template labels (Tzourio-Mazoyer et al., 2002), including both medial OFC and rectus. This analysis confirmed that risk tolerance had a significant association with only the tract strength between right amygdala and ventral mPFC ($r = -0.242$, $p = 0.013$ for right hemisphere; $r = -0.132$, $p = 0.179$ for left hemisphere).

We then examined the relationship between risk tolerance and amygdala structure. Amygdala GMV in each hemisphere was significantly positively correlated with risk tolerance (left amygdala, $r = 0.343$, $p = 0.0004$; right amygdala, $r = 0.270$, $p = 0.0057$; Figure 5). Greater amygdala GMV was associated with higher risk tolerance.

One potential concern is that we may have pursued a different set of connectivity analyses, leading to a different set of findings, had we examined the different imaging modalities in a different order. Reassuringly, though, a whole-brain analysis of GMV also highlights the amygdala, further justifying our focus above on amygdala structural and functional connectivity. A whole-brain analysis revealed that GMV in bilateral amygdalae had the strongest associations with risk tolerance, in the same way that the node strengths of bilateral amygdalae had the strongest associations with risk tolerance (Figure S1). Therefore, regardless of data modality we initially use for data-driven analyses, individuals' risk tolerance has a stronger association with the functional and structural features of amygdala than with any other brain region.

Given previous reports of a positive relationship between risk tolerance and GMV in the right posterior parietal cortex (rPPC) (Gilaie-Dotan et al., 2014; Grubb et al., 2016), we also conducted an ROI analysis to test whether this previously reported association replicates in the present sample. Consistent with previous studies, this ROI analysis revealed a positive association between rPPC GMV and risk tolerance ($r = 0.174$, $p = 0.078$), though this relationship was not significant in our data.

Next, we confirmed that none of our results depend on the specific functional form of risk tolerance that we used. We regressed each of the amygdala features above against (1) risk aversion parameters from two forms of risk-return/mean-variance model,

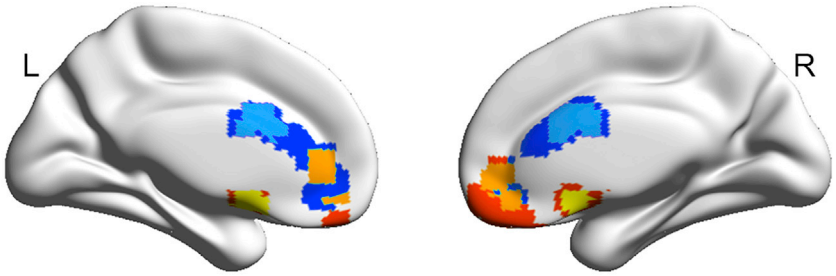

Figure 3. Brain Regions Showing Significant Correlations between Risk Tolerance and Resting-State Functional Connectivity to the Amygdala

Risk tolerance was significantly positively correlated with RSFC between left amygdala and mPFC/ACC (at a height $p < 0.001$ [sky] or 0.005 [blue]) and RSFC between right amygdala and mPFC/rectus (at a height $p < 0.001$ [yellow] or 0.005 [red]). These clusters, identified at a height $p < 0.005$ and an extent corrected $p < 0.05$, partially overlapped (orange).

an alternative to the expected utility model (Markowitz, 1959; Weber et al., 2004) and (2) the percentage of risky choices, as a model-free estimate of risk attitudes. There was a strong correspondence between the risk tolerances estimated from the expected utility model and both the risk aversion parameters estimated from the risk-return models ($r = -0.93$ and -0.92 for the classic and Weber formulations of risk-return) and the overall percentage of risky choices ($r = 0.92$). Not surprisingly given this correspondence, all of the amygdala features identified above were also significantly correlated with both the risk aversion parameters from the risk-return models and the overall percentage of risky choices (Table 1).

Regression Models Predicting Individual Risk Tolerances from Brain Variables

Finally, we examined whether these various measures of functional connectivity, structural connectivity, and structure each explain independent or overlapping variance in risk tolerance. We did this by performing a linear regression analysis including all of the functional and structural features of the amygdala for a given hemisphere to explain risk tolerance. Of note, significant features in such a model explain variance in risk tolerances over and above that explained by all other features. This is because the t-statistic for a given independent variable in a multiple regression is proportional to the correlation between the dependent variable and that portion of the independent variable that is uncorrelated with the remaining independent variables (Cohen et al., 2003). In a regression analysis for the left hemisphere, RSFC strength and relative GMV (i.e., absolute GMV divided by total intracranial volume) of the left amygdala were significant predictors of risk tolerance ($p < 0.05$; Table 2). In a regression analysis for the right hemisphere, RSFC strength, relative GMV, and tract strength of the right amygdala were significant predictors for risk tolerance ($p < 0.05$; Table 2). These regressions show that each of these different measures account for unique variance in risk tolerances.

We also ran linear regressions with each of the measures individually to allow for a comparison of the variance explained by each measure. The amount of variance explained (R^2) was 0.070 for node strength alone, 0.188 for RSFC alone, 0.101 for GMV alone, and 0.020 for tract strength alone for left hemisphere (compared to 0.274 for the combined model); these values were 0.065, 0.183, 0.065, and 0.077 for the respective variables in the right hemisphere (compared to 0.273 for the combined model). Though RSFC appears to explain the most variance in risk tolerance, we caution against this interpretation as this measure is the only one that involves a degree of selection (the MPFC region was selected based on the peak RSFC correlation with risk tolerance) rather than using effects calculated in pre-determined ROIs. However, these results do further reinforce the conclusion that RSFC, GMV, and tract strength (in the right hemisphere) account for unique variance in risk tolerance, as the coefficients on these variables does not change dramatically when all of the variables are included in the regression and the total variance explained is near additive when considering these variables separately and together.

DISCUSSION

To identify neural markers of risk tolerance, we examined the relationship between an individual's risk tolerance and multimodal, context-independent, brain measures, including functional connectivity from RS-fMRI, structural connectivity from DTI, and structural features (specifically, GMV) from T1 anatomical imaging, in a large sample of healthy young adults. We found several intrinsic functional and structural brain markers of risk tolerances. Individuals who were more tolerant of risk showed greater overall connectivity (node strength) of the amygdala, specific increases in RSFC between the amygdala and mPFC, reduced WM tract strength between the amygdala and mPFC, and larger GMV in the amygdala. Of these measures, amygdala-mPFC RSFC and amygdala GMV for each hemisphere made the largest contributions to predicting risk tolerance. These results identify multiple intrinsic structural and functional features of the amygdala that are associated with individual differences in risk tolerance.

Our investigation focused solely on tolerance for risk (a form of uncertainty when the probability of each possible outcome is known), under conditions where only positive outcomes (i.e., winning money) were possible. As such, our data do not speak directly to whether structural and functional features of the amygdala and amygdala-mPFC connectivity are related to individual differences in tolerance for ambiguity (a form of uncertainty when the probability of each possible outcome is unknown; Ellsberg, 1961), risk tolerance for losses (which can differ from that of gains; Kahneman and Tversky, 1979), or loss aversion (the relative weighting of gains and losses; Kahneman and Tversky, 1979). Future research is thus needed to determine whether the markers we have noted are also associated with other individual differences in decision making under uncertainty, or are rather unique to risk tolerance in the domain of gains. Previous work, however, suggests that the amygdala

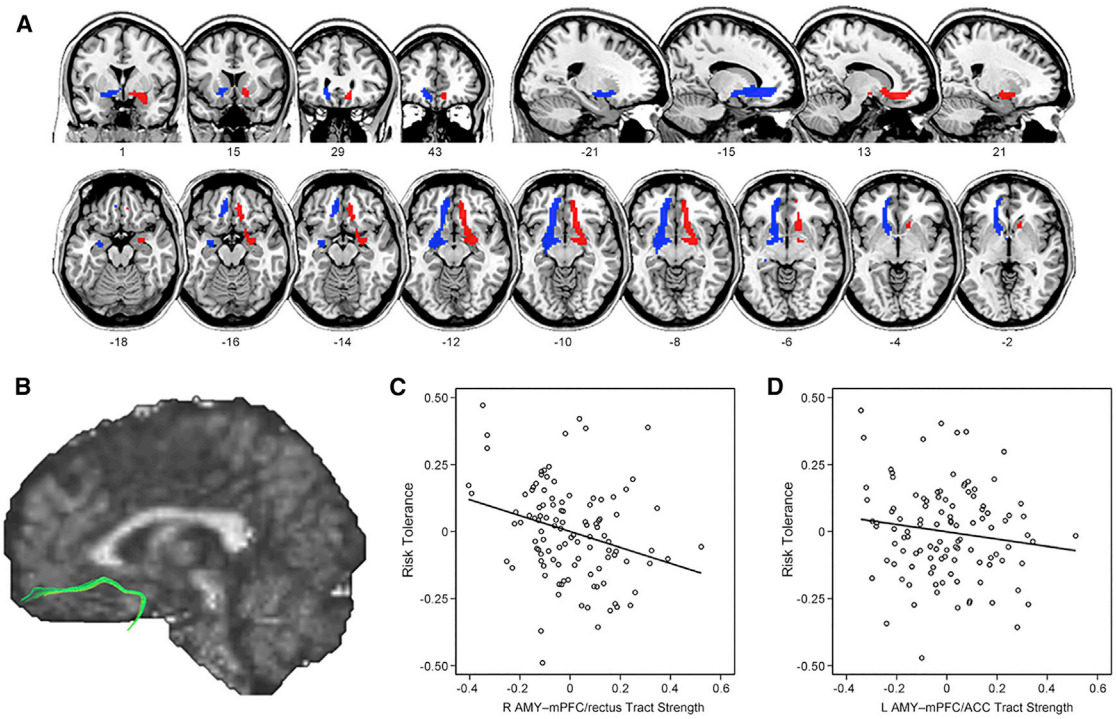

Figure 4. Results from Structural Connectivity Analyses

(A) Group probability maps of amygdala to mPFC white matter tracts (blue for left hemisphere; red for right hemisphere) are illustrated in coronal, sagittal, and axial views. For illustration purposes, individual subject's probabilistic tractography results were transformed into standard space, binarized, and summed across all subjects. Finally, the summed tract images were thresholded to show only overlapping pathways in at least 54 of 108 participants.

(B) A single subject map of amygdala to mPFC tract identified using deterministic tractography (for illustration purposes only).

(C) Partial correlation scatterplot between risk tolerance and tract strength from right amygdala to mPFC/rectus.

(D) Partial correlation scatterplot between risk tolerance and tract strength from left amygdala to mPFC/ACC. For illustration purposes, (C) and (D) were generated by performing Pearson correlation analysis between residuals after regressing out age, sex, and IQ.

and amygdala-mPFC interactions play a more general role in decision making and learning, for both gains and losses. For example, task-induced functional activity in amygdala reflects the value of both risky and ambiguous outcomes (Levy et al., 2010) or the degree of uncertainty (ambiguity > risk; Hsu et al., 2005) during decision making under uncertainty and is associated with risk (Huettel et al., 2006) or loss avoidance (Sokol-Hessner et al., 2009) and with the effect of loss-gain framing (De Martino et al., 2006). These findings are consistent with extensive work in animal models demonstrating an important role for the amygdala, and amygdala-mPFC interactions, in the evaluation of potential future outcomes during learning and decision making (Floresco et al., 2008; Murray and Wise, 2010). Anatomical tracing studies have identified robust bidirectional connections between the amygdala and mPFC (Amaral and Price, 1984; Croxson et al., 2005; Kim et al., 2016). The firing of neurons in both regions reflects the value of expected outcomes during reward learning (Baxter and Murray, 2002; Schultz et al., 2008; Morrison et al., 2011), lesioning one of these regions disrupts the value signals in the other (Rudebeck et al., 2013), and disrupting the connection between these regions impairs flexible reward learning (Chau et al., 2015). Researchers have suggested that these two regions make dissociable contributions to reinforcement learning, with the amygdala being important for forming cue-outcome associations/expectancies, and the OFC/mPFC using such reward expectancy information to guide behavior in a way that enhances or inhibits stimulus-driven responses mediated by the amygdala (Pickens et al., 2003; Holland and Gallagher, 2004). In line with this notion, neuroimaging studies of reward-related choice and learning in humans have also revealed differential contributions of the amygdala and mPFC to reward expectancy and behavioral choice (Arana et al., 2003; Hampton et al., 2007). For example, Arana et al. (2003) showed that the amygdala activity covaried with the subjective incentive value of foods regardless of whether a choice was required, whereas the mPFC activity correlated with the value when making a choice.

Our findings linking structural and functional features of the amygdala and amygdala-prefrontal interactions to risk tolerance are also broadly consistent with recent work linking the same markers with anxiety. The amygdala is well known to be important in processing fear and threat (Adolphs, 2008), as well as uncertainty-related anxiety (Grupe and Nitschke, 2013). For example, uncertain anticipation of negative emotional pictures recruits the amygdala (Sarinopoulos et al., 2010) and such amygdala activation is increased in patients with anxiety disorders relative to healthy individuals (Williams et al., 2015). Additionally, patients with anxiety disorders show heightened resting

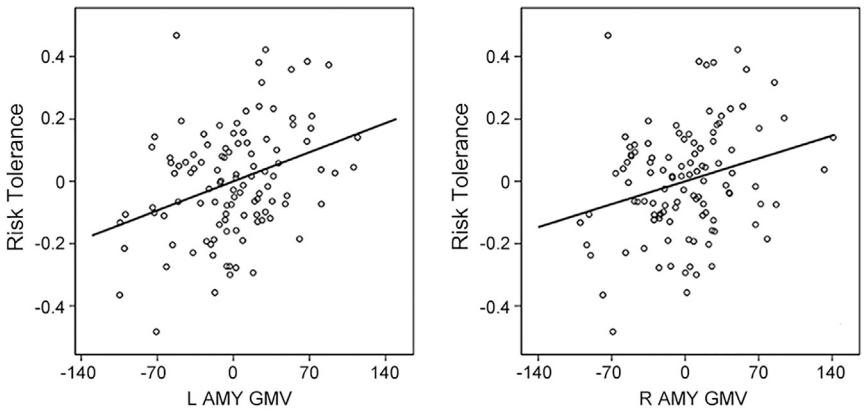

Figure 5. Partial Correlation Scatterplot between Risk Tolerance and Amygdala Gray Matter Volume

For illustration purposes, this scatterplot was generated by performing Pearson correlation analysis between residuals after regressing out age, sex, IQ, and total intracranial volume.

metabolic activity in the amygdala (Semple et al., 2000; Furmark et al., 2002). The reciprocal connections between the amygdala and mPFC play a critical role in fear learning and extinction (Marek et al., 2013), as well as the emotional regulation of negative affect (Banks et al., 2007; Pessoa, 2008; Motzkin et al., 2015), and have been implicated in anxiety. Individuals with a genetic predisposition to anxiety exhibit not only increased amygdala activation during processing of negative emotion, but also reduced amygdala volume and reduced amygdala-mPFC functional connectivity (Pezawas et al., 2005). Indeed, lower amygdala-mPFC RSFC is correlated with higher state anxiety scores in healthy individuals (Kim et al., 2011) and higher anxiety severity in patients with anxiety disorders (Dodhia et al., 2014; though see Satterthwaite et al., 2016). Previous DTI studies have also reported that higher FA in amygdala-mPFC tract was correlated with higher trait anxiety levels (Clewett et al., 2014; Modi et al., 2013), though other studies have reported the opposite association (Kim and Whalen, 2009; Kim et al., 2016). Thus, the direction of the associations that we observed between risk aversion and amygdala GMV, amygdala-mPFC RSFC, and amygdala-mPFC WM tract strength are similar to those previously identified between these markers and anxiety. This demonstrates that these same markers extend to predicting the avoidance of risky options during decision making.

Given evidence that risk tolerance evolves with age (Tymula et al., 2013; Grubb et al., 2016), it is interesting to note that functional and structural connectivity between the amygdala and mPFC also exhibits age-related changes, showing an increase in positive RSFC (Gabard-Durnam et al., 2014) and a decline in the coherence of fibers between these two regions from adolescent to young adults (Burzynska et al., 2010; Clewett et al., 2014). Furthermore, from young adulthood to old age, the relationship between functional and structural connectivity between amygdala and mPFC evolves, switching from negative functional-structural connectivity coupling (as we observe here) to positive coupling (Ford and Kensinger, 2014; though see Hagmann et al., 2010). Task-based functional connectivity during emotional processing also exhibits developmental effects, shifting from positive amygdala-mPFC connectivity to negative connectivity from childhood through young adulthood (Gee et al., 2013; Wu et al., 2016), which has been interpreted as evidence that bottom-up signals from amygdala to mPFC emerge earlier than top-down regulatory control of mPFC on amygdala (Etkin et al., 2011; Gee et al., 2013; Wu et al., 2016). An interesting question for future research will be whether age-related changes in amygdala-mPFC structural and functional connectivity mediate changes in risk tolerance over the lifespan, as has recently been argued for another brain marker of risk tolerance, GMV in the right posterior parietal cortex (Gilaie-Dotan et al., 2014; Grubb et al., 2016).

Although previously noted in young adults (Ford and Kensinger, 2014), the inverse relationship we observed between functional and structural amygdala-mPFC connectivity is not immediately intuitive. One possibility is that more effective communication between the amygdala and mPFC (as indexed by higher RSFC) may depend on pruning the structural connections between the two regions (as indexed by lower probabilistic tract strength). Another possibility is that the two measures may differentially weight amygdala-to-mPFC versus mPFC-to-amygdala projections, and projections of different directionality may play opposite roles in promoting risk tolerance. An important aim for future research should be to understand the undoubtedly complex relationship between RSFC and probabilistic tractography measures.

Though most of our brain markers, including node strength, RSFC, and GMV, were significant for both the right and left amygdala, the association between risk tolerance and amygdala-mPFC tract strength was significant only in right hemisphere. Though we did not have hypotheses about hemispheric lateralization, much previous work has suggested potential hemispheric specialization of the human amygdala. Previous studies have argued that the right amygdala is more involved in avoidance behavior and the left in approach, the right is more involved in negative emotions and the left in positive (Baker and Kim, 2004; Coleman-Mesches and McGaugh 1995), the right in formation of emotional memory and the left in retrieval (Sergerie et al., 2006), and the right in rapid emotional processing and the left in more elaborative (Sergerie et al., 2008). The lateralization of functional or structural connections between the amygdala and mPFC is less well studied, though two recent studies have found that amygdala-mPFC WM tract strength in the right hemisphere is more strongly associated with anxiety than the left (Eden et al., 2015; Kim et al., 2016).

To our knowledge, this is the highest-powered study to date to investigate the multimodal (context-independent) neural markers of risk tolerance. We found that structural features of the amygdala, and functional and structural connectivity between the amygdala and mPFC, predicted risk tolerance. The direction of these associations with risk aversion matches that

Table 1. Summary of Regression Analyses between Each of Brain Measures and Alternative Risk Estimates

	Expected Utility Model	The Percentages (%) of Participants' Choices				Mean-Variance Model	
	risk tolerance	% of risky choices over all probability	% of risky choices on small probabilities	% of risky choices on intermediate probabilities	% of risky choices on large probabilities	Markowitz's risk-return parameter	Weber's risk-return parameter
Association with the node strength of amygdala							
Left hemisphere	r = 0.265, p = 0.007*	r = 0.256, p = 0.009*	r = 0.154, p = 0.118	r = 0.256, p = 0.009*	r = 0.135, p = 0.173	r = −0.226, p = 0.021*	r = −0.270, p = 0.006*
Right hemisphere	r = 0.261, p = 0.007*	r = 0.262, p = 0.007*	r = 0.176, p = 0.073	r = 0.266, p = 0.006*	r = 0.119, p = 0.230	r = −0.227, p = 0.021*	r = −0.270, p = 0.006*
Association with functional connectivity between amygdala and MPFC							
Left hemisphere	r = 0.434, p < 0.001*	r = 0.406, p < 0.001*	r = 0.249, p = 0.011*	r = 0.423, p < 0.001*	r = 0.171, p = 0.083	r = −0.397, p < 0.001*	r = −0.392, p < 0.001*
Right hemisphere	r = 0.424, p < 0.001*	r = 0.414, p < 0.001*	r = 0.316, p = 0.001*	r = 0.400, p < 0.001*	r = 0.213, p = 0.030*	r = −0.367, p < 0.001*	r = −0.336, p < 0.001*
Association with white matter tract strength between amygdala and MPFC							
Left hemisphere	r = −0.140, p = 0.155	r = −0.082, p = 0.406	r = −0.170, p = 0.084	r = −0.140, p = 0.153	r = 0.197, p = 0.044*	r = 0.147, p = 0.135	r = 0.108, p = 0.271
Right hemisphere	r = −0.278, p = 0.004*	r = −0.238, p = 0.015*	r = −0.209, p = 0.033*	r = −0.290, p = 0.003*	r = 0.049, p = 0.617	r = 0.234, p = 0.016*	r = 0.260, p = 0.007*
Association with GMV in amygdala							
Left hemisphere	r = 0.343, p = 0.001*	r = 0.269, p = 0.006*	r = 0.298, p = 0.002*	r = 0.268, p = 0.006*	r = 0.054, p = 0.586	r = −0.323, p = 0.001*	r = −0.309, p = 0.001*
Right hemisphere	r = 0.270, p = 0.006*	r = 0.182, p = 0.065	r = 0.237, p = 0.015*	r = 0.187, p = 0.058	r = 0.001, p = 0.994	r = −0.224, p = 0.022*	r = −0.225, p = 0.022*

*p < 0.05.

Table 2. Summary of Linear Regression Models with Each of the Measures Individually and Together

	Model with Only Node Strength	Model with Only RSFC	Model with Only GMV	Model with Only Tract Strength	Model with All Brain Variables
Model for left amygdala					
Constant	−8.79E-12 (0.017)	−2.21E-10 (0.016)	6.280E-12 (0.016)	−9.26E-12 (0.017)	−2.04E-10 (0.015)
Node strength	0.008 (0.003)**	–	–	–	−0.001 (0.003)
RSFC	–	0.652 (0.131)***	–	–	0.645 (166)***
GMV	–	–	1.678 (0.487)**	–	1.552 (0.446)**
Tract strength	–	–	–	−0.141 (0.097)	−0.003 (0.089)
R^2	0.07	0.188	0.101	0.02	0.274
Model for right amygdala					
Constant	−1.03E-11 (0.017)	1.070E-11 (0.016)	6.762E-11 (0.017)	−4.51E-08 (0.017)	−3.25E-08 (0.015)
Node strength	0.008 (0.003)**	–	–	–	0.004 (0.003)
RSFC	–	0.719 (0.147)***	–	–	0.537 (0.163)**
GMV	–	–	1.384 (0.510)**	–	1.087 (0.462)*
Tract strength	–	–	–	−0.296 (0.099) **	−0.214 (0.092)*
R^2	0.065	0.183	0.065	0.077	0.273

Data are given as unstandardized coefficients, B (standard errors). Coefficients significantly different from zero indicated by asterisks: *p < 0.05; **p < 0.01;***p < 0.001. RSFC, resting-state functional connectivity; GMV, gray matter volume; R^2, the amount of variance explained by the model.

observed previously between these same markers and anxiety. These results further reinforce a key role for interactions between amygdala and mPFC in value-based decision making, particularly in the context of risk. Based on these results, to the extent that experimental manipulations (such as lesions or brain stimulation) altered functional or structural connectivity between amygdala and mPFC, we would expect that these manipulations also change risk tolerance in the according direction. In addition, if further refined and validated, the biomarkers observed here might someday prove useful in predicting individual differences in risk tolerance and risk-taking behavior.

STAR★METHODS

Detailed methods are provided in the online version of this paper and include the following:

- KEY RESOURCES TABLE
- CONTACT FOR REAGENT AND RESOURCE SHARING
- EXPERIMENTAL MODEL AND SUBJECT DETAILS
  - Participants
- METHOD DETAILS
  - Risk tolerance task
  - Image acquisition
- QUANTIFICATION AND STATISTICAL ANALYSIS
  - RS-fMRI analysis
  - DTI analysis
  - T1-MRI analysis
  - Linear regression analysis to estimate brain predictors of risk tolerance
- DATA AND SOFTWARE AVAILABILITY

SUPPLEMENTAL INFORMATION

Supplemental Information includes one figure and can be found with this article online at https://doi.org/10.1016/j.neuron.2018.03.019.

ACKNOWLEDGMENTS

This study was supported by National Cancer Institute grants R01 CA170297 (J.K. and C.L.) and R35 CA197461 (C.L.) and National Institute of Drug Abuse grant R01 DA029149 (J.K.). We thank Trishala Parthasarathi, Mairead McConnell, Nicole Cooper, Katie Caulfield, and Leah Bernardo for their assistance in project management and the following individuals for their assistance in data collection: Kalijah Terilli, Dominique Spence, Hyoun Ju Sohn, Rachel Sharp, Maura Schlussel, Sarah Price, Dahlia Mukherjee, Rickie Miglin, Jeffrey Luery, Rebecca Kazinka, Jennifer Jorgensen, Gabriel Donnay, and Anne Marie Burke. We also thank Dr. Yangming Ou for helpful technical comments regarding RAVENS analysis using DRAMMS, and Dr. Ifat Levy and Dr. Theodore D. Satterthwaite for helpful comments on an early draft of the manuscript.

AUTHOR CONTRIBUTIONS

C.L. and J.W.K. designed the research. W.H.J. and S.L. analyzed the data. All authors discussed the analyses, results, and interpretation, and wrote the manuscript.

DECLARATION OF INTERESTS

The authors declare no competing interests.

Received: September 16, 2017
Revised: January 21, 2018
Accepted: March 10, 2018
Published: April 5, 2018

REFERENCES

Adolphs, R. (2008). Fear, faces, and the human amygdala. Curr. Opin. Neurobiol. *18*, 166–172.

Amaral, D.G., and Price, J.L. (1984). Amygdalo-cortical projections in the monkey (Macaca fascicularis). J. Comp. Neurol. *230*, 465–496.

Anderson, L.R., and Mellor, J.M. (2008). Predicting health behaviors with an experimental measure of risk preference. J. Health Econ. *27*, 1260–1274.

Arana, F.S., Parkinson, J.A., Hinton, E., Holland, A.J., Owen, A.M., and Roberts, A.C. (2003). Dissociable contributions of the human amygdala and

orbitofrontal cortex to incentive motivation and goal selection. J. Neurosci. *23*, 9632–9638.

Baker, K.B., and Kim, J.J. (2004). Amygdalar lateralization in fear conditioning: evidence for greater involvement of the right amygdala. Behav. Neurosci. *118*, 15–23.

Banks, S.J., Eddy, K.T., Angstadt, M., Nathan, P.J., and Phan, K.L. (2007). Amygdala-frontal connectivity during emotion regulation. Soc. Cogn. Affect. Neurosci. *2*, 303–312.

Barfoed, B.L., Paulsen, M.S., Christensen, P.M., Halvorsen, P.A., Kjær, T., Larsen, M.L., Larsen, P.V., Nielsen, J.B., Søndergaard, J., and Jarbøl, D.E. (2016). Associations between patients' risk attitude and their adherence to statin treatment - a population based questionnaire and register study. BMC Fam. Pract. *17*, 28.

Barsky, R.B., Juster, F.T., Kimball, M.S., and Shapiro, M.D. (1997). Preference parameters and behavioral heterogeneity: An experimental approach in the Health and Retirement Study. Q. J. Econ. *112*, 537–579.

Baxter, M.G., and Murray, E.A. (2002). The amygdala and reward. Nat. Rev. Neurosci. *3*, 563–573.

Behrens, T.E., Woolrich, M.W., Jenkinson, M., Johansen-Berg, H., Nunes, R.G., Clare, S., Matthews, P.M., Brady, J.M., and Smith, S.M. (2003). Characterization and propagation of uncertainty in diffusion-weighted MR imaging. Magn. Reson. Med. *50*, 1077–1088.

Behrens, T.E., Berg, H.J., Jbabdi, S., Rushworth, M.F., and Woolrich, M.W. (2007). Probabilistic diffusion tractography with multiple fibre orientations: What can we gain? Neuroimage *34*, 144–155.

Behzadi, Y., Restom, K., Liau, J., and Liu, T.T. (2007). A component based noise correction method (CompCor) for BOLD and perfusion based fMRI. Neuroimage *37*, 90–101.

Branas-Garza, P., Georgantzìs, N., and Guillen, P. (2007). Direct and indirect effects of pathological gambling on risk attitudes. Judgm. Decis. Mak. *2*, 126–136.

Burzynska, A.Z., Preuschhof, C., Bäckman, L., Nyberg, L., Li, S.C., Lindenberger, U., and Heekeren, H.R. (2010). Age-related differences in white matter microstructure: region-specific patterns of diffusivity. Neuroimage *49*, 2104–2112.

Chau, B.K., Sallet, J., Papageorgiou, G.K., Noonan, M.P., Bell, A.H., Walton, M.E., and Rushworth, M.F. (2015). Contrasting roles for orbitofrontal cortex and amygdala in credit assignment and learning in macaques. Neuron *87*, 1106–1118.

Clewett, D., Bachman, S., and Mather, M. (2014). Age-related reduced prefrontal-amygdala structural connectivity is associated with lower trait anxiety. Neuropsychology *28*, 631–642.

Cocchi, L., Bramati, I.E., Zalesky, A., Furukawa, E., Fontenelle, L.F., Moll, J., Tripp, G., and Mattos, P. (2012). Altered functional brain connectivity in a non-clinical sample of young adults with attention-deficit/hyperactivity disorder. J. Neurosci. *32*, 17753–17761.

Cohen, J., Cohen, P., West, S.G., and Aiken, L.S. (2003). Applied Multiple Regression/Correlation Analysis for the Behavioral Sciences, Third Edition (Lawrence Erlbaum).

Coleman-Mesches, K., and McGaugh, J.L. (1995). Differential involvement of the right and left amygdalae in expression of memory for aversively motivated training. Brain Res. *670*, 75–81.

Croxson, P.L., Johansen-Berg, H., Behrens, T.E., Robson, M.D., Pinsk, M.A., Gross, C.G., Richter, W., Richter, M.C., Kastner, S., and Rushworth, M.F. (2005). Quantitative investigation of connections of the prefrontal cortex in the human and macaque using probabilistic diffusion tractography. J. Neurosci. *25*, 8854–8866.

Cui, Z., Zhong, S., Xu, P., He, Y., and Gong, G. (2013). PANDA: a pipeline toolbox for analyzing brain diffusion images. Front. Hum. Neurosci. *7*, 42.

Davatzikos, C., Genc, A., Xu, D., and Resnick, S.M. (2001). Voxel-based morphometry using the RAVENS maps: methods and validation using simulated longitudinal atrophy. Neuroimage *14*, 1361–1369.

De Martino, B., Kumaran, D., Seymour, B., and Dolan, R.J. (2006). Frames, biases, and rational decision-making in the human brain. Science *313*, 684–687.

De Martino, B., Camerer, C.F., and Adolphs, R. (2010). Amygdala damage eliminates monetary loss aversion. Proc. Natl. Acad. Sci. USA *107*, 3788–3792.

Dodhia, S., Hosanagar, A., Fitzgerald, D.A., Labuschagne, I., Wood, A.G., Nathan, P.J., and Phan, K.L. (2014). Modulation of resting-state amygdala-frontal functional connectivity by oxytocin in generalized social anxiety disorder. Neuropsychopharmacology *39*, 2061–2069.

Dohmen, T., Falk, A., Huffmann, D., Sunde, U., Schupp, J., and Wagner G. (2005). Individual Risk Attitudes: New Evidence from a Large, Representative, Experimentally-Validated Survey. (IZA Discussion Papers No. 1730).

Eden, A.S., Schreiber, J., Anwander, A., Keuper, K., Laeger, I., Zwanzger, P., Zwitserlood, P., Kugel, H., and Dobel, C. (2015). Emotion regulation and trait anxiety are predicted by the microstructure of fibers between amygdala and prefrontal cortex. J. Neurosci. *35*, 6020–6027.

Ekelund, J., Johansson, E., Jarvelin, M., and Lichtermann, D. (2005). Self-Employment and Risk Aversion – Evidence from Psychological Test Data. Labour Econ. *12*, 649–659.

Eklund, A., Nichols, T.E., and Knutsson, H. (2016). Cluster failure: Why fMRI inferences for spatial extent have inflated false-positive rates. Proc. Natl. Acad. Sci. USA *113*, 7900–7905.

Ellsberg, D. (1961). Risk, ambiguity, and the Savage axioms. Q. J. Econ. *175*, 643–669.

Ernst, M., Nelson, E.E., McClure, E.B., Monk, C.S., Munson, S., Eshel, N., Zarahn, E., Leibenluft, E., Zametkin, A., Towbin, K., et al. (2004). Choice selection and reward anticipation: an fMRI study. Neuropsychologia *42*, 1585–1597.

Etkin, A., Egner, T., and Kalisch, R. (2011). Emotional processing in anterior cingulate and medial prefrontal cortex. Trends Cogn. Sci. *15*, 85–93.

Floresco, S.B., St Onge, J.R., Ghods-Sharifi, S., and Winstanley, C.A. (2008). Cortico-limbic-striatal circuits subserving different forms of cost-benefit decision making. Cogn. Affect. Behav. Neurosci. *8*, 375–389.

Ford, J.H., and Kensinger, E.A. (2014). The relation between structural and functional connectivity depends on age and on task goals. Front. Hum. Neurosci. *8*, 307.

Fraenkel, L., Bogardus, S.T., Jr., and Wittink, D.R. (2003). Risk-attitude and patient treatment preferences. Lupus *12*, 370–376.

Fumagalli, R. (2014). Neural findings and economic models: why brains have limited relevance for economics. Philos. Soc. Sci. *44*, 606–629.

Furmark, T., Tillfors, M., Marteinsdottir, I., Fischer, H., Pissiota, A., Långström, B., and Fredrikson, M. (2002). Common changes in cerebral blood flow in patients with social phobia treated with citalopram or cognitive-behavioral therapy. Arch. Gen. Psychiatry *59*, 425–433.

Gabard-Durnam, L.J., Flannery, J., Goff, B., Gee, D.G., Humphreys, K.L., Telzer, E., Hare, T., and Tottenham, N. (2014). The development of human amygdala functional connectivity at rest from 4 to 23 years: a cross-sectional study. Neuroimage *95*, 193–207.

Gee, D.G., Humphreys, K.L., Flannery, J., Goff, B., Telzer, E.H., Shapiro, M., Hare, T.A., Bookheimer, S.Y., and Tottenham, N. (2013). A developmental shift from positive to negative connectivity in human amygdala-prefrontal circuitry. J. Neurosci. *33*, 4584–4593.

Gilaie-Dotan, S., Tymula, A., Cooper, N., Kable, J.W., Glimcher, P.W., and Levy, I. (2014). Neuroanatomy predicts individual risk attitudes. J. Neurosci. *34*, 12394–12401.

Glimcher, P.W. (2008). Understanding risk: a guide for the perplexed. Cogn. Affect. Behav. Neurosci. *8*, 348–354.

Grubb, M.A., Tymula, A., Gilaie-Dotan, S., Glimcher, P.W., and Levy, I. (2016). Neuroanatomy accounts for age-related changes in risk preferences. Nat. Commun. *7*, 13822.

Grupe, D.W., and Nitschke, J.B. (2013). Uncertainty and anticipation in anxiety: an integrated neurobiological and psychological perspective. Nat. Rev. Neurosci. *14*, 488–501.

Hagmann, P., Sporns, O., Madan, N., Cammoun, L., Pienaar, R., Wedeen, V.J., Meuli, R., Thiran, J.P., and Grant, P.E. (2010). White matter maturation reshapes structural connectivity in the late developing human brain. Proc. Natl. Acad. Sci. USA *107*, 19067–19072.

Hampton, A.N., Adolphs, R., Tyszka, M.J., and O'Doherty, J.P. (2007). Contributions of the amygdala to reward expectancy and choice signals in human prefrontal cortex. Neuron *55*, 545–555.

Holland, P.C., and Gallagher, M. (2004). Amygdala-frontal interactions and reward expectancy. Curr. Opin. Neurobiol. *14*, 148–155.

Hsu, M., Bhatt, M., Adolphs, R., Tranel, D., and Camerer, C.F. (2005). Neural systems responding to degrees of uncertainty in human decision-making. Science *310*, 1680–1683.

Huang, Y.F., Soon, C.S., Mullette-Gillman, O.A., and Hsieh, P.J. (2014). Preexisting brain states predict risky choices. Neuroimage *101*, 466–472.

Huettel, S.A., Stowe, C.J., Gordon, E.M., Warner, B.T., and Platt, M.L. (2006). Neural signatures of economic preferences for risk and ambiguity. Neuron *49*, 765–775.

Johansen-Berg, H., and Rushworth, M.F. (2009). Using diffusion imaging to study human connectional anatomy. Annu. Rev. Neurosci. *32*, 75–94.

Kable, J.W., and Levy, I. (2015). Neural markers of individual differences in decision-making. Curr. Opin. Behav. Sci. *5*, 100–107.

Kable, J.W., Caulfield, M.K., Falcone, M., McConnell, M., Bernardo, L., Parthasarathi, T., Cooper, N., Ashare, R., Audrain-McGovern, J., Hornik, R., et al. (2017). No effect of commercial cognitive training on brain activity, choice behavior, or cognitive performance. J. Neurosci. *37*, 7390–7402.

Kahneman, D., and Tversky, A. (1979). Prospect theory: an analysis of decision under risk. Econometrica *47*, 263–292.

Kim, M.J., and Whalen, P.J. (2009). The structural integrity of an amygdala-prefrontal pathway predicts trait anxiety. J. Neurosci. *29*, 11614–11618.

Kim, M.J., Gee, D.G., Loucks, R.A., Davis, F.C., and Whalen, P.J. (2011). Anxiety dissociates dorsal and ventral medial prefrontal cortex functional connectivity with the amygdala at rest. Cereb. Cortex *21*, 1667–1673.

Kim, M.J., Brown, A.C., Mattek, A.M., Chavez, S.J., Taylor, J.M., Palmer, A.L., Wu, Y.C., and Whalen, P.J. (2016). The inverse relationship between the microstructural variability of amygdala-prefrontal pathways and trait anxiety is moderated by sex. Front. Syst. Neurosci. *10*, 93.

Knutson, B., and Huettel, S.A. (2015). The risk matrix. Curr. Opin. Behav. Sci. *5*, 141–146.

Krain, A.L., Gotimer, K., Hefton, S., Ernst, M., Castellanos, F.X., Pine, D.S., and Milham, M.P. (2008). A functional magnetic resonance imaging investigation of uncertainty in adolescents with anxiety disorders. Biol. Psychiatry *63*, 563–568.

Kuhnen, C.M., and Knutson, B. (2005). The neural basis of financial risk taking. Neuron *47*, 763–770.

Lejuez, C.W., Aklin, W.M., Jones, H.A., Richards, J.B., Strong, D.R., Kahler, C.W., and Read, J.P. (2003). The Balloon Analogue Risk Task (BART) differentiates smokers and nonsmokers. Exp. Clin. Psychopharmacol. *11*, 26–33.

Lejuez, C.W., Aklin, W., Bornovalova, M., and Moolchan, E.T. (2005). Differences in risk-taking propensity across inner-city adolescent ever- and never-smokers. Nicotine Tob. Res. *7*, 71–79.

Leong, J.K., Pestilli, F., Wu, C.C., Samanez-Larkin, G.R., and Knutson, B. (2016). White-Matter Tract Connecting Anterior Insula to Nucleus Accumbens Correlates with Reduced Preference for Positively Skewed Gambles. Neuron *89*, 63–69.

Levy, I., Snell, J., Nelson, A.J., Rustichini, A., and Glimcher, P.W. (2010). Neural representation of subjective value under risk and ambiguity. J. Neurophysiol. *103*, 1036–1047.

Lynall, M.E., Bassett, D.S., Kerwin, R., McKenna, P.J., Kitzbichler, M., Muller, U., and Bullmore, E. (2010). Functional connectivity and brain networks in schizophrenia. J. Neurosci. *30*, 9477–9487.

Marek, R., Strobel, C., Bredy, T.W., and Sah, P. (2013). The amygdala and medial prefrontal cortex: partners in the fear circuit. J. Physiol. *591*, 2381–2391.

Markowitz, H.M. (1959). Portfolio Selection: Efficient Diversification of Investments (John Wiley & Sons).

Modi, S., Trivedi, R., Singh, K., Kumar, P., Rathore, R.K., Tripathi, R.P., and Khushu, S. (2013). Individual differences in trait anxiety are associated with white matter tract integrity in fornix and uncinate fasciculus: preliminary evidence from a DTI based tractography study. Behav. Brain Res. *238*, 188–192.

Mohr, P.N., Biele, G., and Heekeren, H.R. (2010). Neural processing of risk. J. Neurosci. *30*, 6613–6619.

Morrison, S.E., Saez, A., Lau, B., and Salzman, C.D. (2011). Different time courses for learning-related changes in amygdala and orbitofrontal cortex. Neuron *71*, 1127–1140.

Motzkin, J.C., Philippi, C.L., Wolf, R.C., Baskaya, M.K., and Koenigs, M. (2015). Ventromedial prefrontal cortex is critical for the regulation of amygdala activity in humans. Biol. Psychiatry *77*, 276–284.

Murray, E.A., and Wise, S.P. (2010). Interactions between orbital prefrontal cortex and amygdala: advanced cognition, learned responses and instinctive behaviors. Curr. Opin. Neurobiol. *20*, 212–220.

Ou, Y., Sotiras, A., Paragios, N., and Davatzikos, C. (2011). DRAMMS: Deformable registration via attribute matching and mutual-saliency weighting. Med. Image Anal. *15*, 622–639.

Pessoa, L. (2008). On the relationship between emotion and cognition. Nat. Rev. Neurosci. *9*, 148–158.

Pezawas, L., Meyer-Lindenberg, A., Drabant, E.M., Verchinski, B.A., Munoz, K.E., Kolachana, B.S., Egan, M.F., Mattay, V.S., Hariri, A.R., and Weinberger, D.R. (2005). 5-HTTLPR polymorphism impacts human cingulate-amygdala interactions: a genetic susceptibility mechanism for depression. Nat. Neurosci. *8*, 828–834.

Pickens, C.L., Saddoris, M.P., Setlow, B., Gallagher, M., Holland, P.C., and Schoenbaum, G. (2003). Different roles for orbitofrontal cortex and basolateral amygdala in a reinforcer devaluation task. J. Neurosci. *23*, 11078–11084.

Power, J.D., Barnes, K.A., Snyder, A.Z., Schlaggar, B.L., and Petersen, S.E. (2012). Spurious but systematic correlations in functional connectivity MRI networks arise from subject motion. Neuroimage *59*, 2142–2154.

Preuschoff, K., Quartz, S.R., and Bossaerts, P. (2008). Human insula activation reflects risk prediction errors as well as risk. J. Neurosci. *28*, 2745–2752.

Roalf, D.R., Quarmley, M., Elliott, M.A., Satterthwaite, T.D., Vandekar, S.N., Ruparel, K., Gennatas, E.D., Calkins, M.E., Moore, T.M., Hopson, R., et al. (2016). The impact of quality assurance assessment on diffusion tensor imaging outcomes in a large-scale population-based cohort. Neuroimage *125*, 903–919.

Rubinov, M., and Sporns, O. (2010). Complex network measures of brain connectivity: uses and interpretations. Neuroimage *52*, 1059–1069.

Rudebeck, P.H., Mitz, A.R., Chacko, R.V., and Murray, E.A. (2013). Effects of amygdala lesions on reward-value coding in orbital and medial prefrontal cortex. Neuron *80*, 1519–1531.

Sarinopoulos, I., Grupe, D.W., Mackiewicz, K.L., Herrington, J.D., Lor, M., Steege, E.E., and Nitschke, J.B. (2010). Uncertainty during anticipation modulates neural responses to aversion in human insula and amygdala. Cereb. Cortex *20*, 929–940.

Satterthwaite, T.D., Cook, P.A., Bruce, S.E., Conway, C., Mikkelsen, E., Satchell, E., Vandekar, S.N., Durbin, T., Shinohara, R.T., and Sheline, Y.I. (2016). Dimensional depression severity in women with major depression and post-traumatic stress disorder correlates with fronto-amygdalar hypoconnectivty. Mol. Psychiatry *21*, 894–902.

Schepis, T.S., McFetridge, A., Chaplin, T.M., Sinha, R., and Krishnan-Sarin, S. (2011). A pilot examination of stress-related changes in impulsivity and risk

taking as related to smoking status and cessation outcome in adolescents. Nicotine Tob. Res. *13*, 611–615.

Schultz, W., Preuschoff, K., Camerer, C., Hsu, M., Fiorillo, C.D., Tobler, P.N., and Bossaerts, P. (2008). Explicit neural signals reflecting reward uncertainty. Philos. Trans. R. Soc. Lond. B Biol. Sci. *363*, 3801–3811.

Semple, W.E., Goyer, P.F., McCormick, R., Donovan, B., Muzic, R.F., Jr., Rugle, L., McCutcheon, K., Lewis, C., Liebling, D., Kowaliw, S., et al. (2000). Higher brain blood flow at amygdala and lower frontal cortex blood flow in PTSD patients with comorbid cocaine and alcohol abuse compared with normals. Psychiatry *63*, 65–74.

Sergerie, K., Lepage, M., and Armony, J.L. (2006). A process-specific functional dissociation of the amygdala in emotional memory. J. Cogn. Neurosci. *18*, 1359–1367.

Sergerie, K., Chochol, C., and Armony, J.L. (2008). The role of the amygdala in emotional processing: a quantitative meta-analysis of functional neuroimaging studies. Neurosci. Biobehav. Rev. *32*, 811–830.

Smith, S.M., Jenkinson, M., Woolrich, M.W., Beckmann, C.F., Behrens, T.E., Johansen-Berg, H., Bannister, P.R., De Luca, M., Drobnjak, I., Flitney, D.E., et al. (2004). Advances in functional and structural MR image analysis and implementation as FSL. Neuroimage *23* (*Suppl 1*), S208–S219.

Sokol-Hessner, P., Hsu, M., Curley, N.G., Delgado, M.R., Camerer, C.F., and Phelps, E.A. (2009). Thinking like a trader selectively reduces individuals' loss aversion. Proc. Natl. Acad. Sci. USA *106*, 5035–5040.

Studer, B., Manes, F., Humphreys, G., Robbins, T.W., and Clark, L. (2015). Risk-sensitive decision-making in patients with posterior parietal and ventromedial prefrontal cortex injury. Cereb. Cortex *25*, 1–9.

Tymula, A., Rosenberg Belmaker, L.A., Ruderman, L., Glimcher, P.W., and Levy, I. (2013). Like cognitive function, decision making across the life span shows profound age-related changes. Proc. Natl. Acad. Sci. USA *110*, 17143–17148.

Tzourio-Mazoyer, N., Landeau, B., Papathanassiou, D., Crivello, F., Etard, O., Delcroix, N., Mazoyer, B., and Joliot, M. (2002). Automated anatomical labeling of activations in SPM using a macroscopic anatomical parcellation of the MNI MRI single-subject brain. Neuroimage *15*, 273–289.

von Neumann, J., and Morgenstern, O. (1994). Theory of Games and Economic Behavior (Princeton University Press).

Wang, J., Zuo, X., and He, Y. (2010). Graph-based network analysis of resting-state functional MRI. Front. Syst. Neurosci. *4*, 16.

Weber, E.U., Shafir, S., and Blais, A.R. (2004). Predicting risk sensitivity in humans and lower animals: risk as variance or coefficient of variation. Psychol. Rev. *111*, 430–445.

Williams, L.E., Oler, J.A., Fox, A.S., McFarlin, D.R., Rogers, G.M., Jesson, M.A., Davidson, R.J., Pine, D.S., and Kalin, N.H. (2015). Fear of the unknown: uncertain anticipation reveals amygdala alterations in childhood anxiety disorders. Neuropsychopharmacology *40*, 1428–1435.

Wu, M., Kujawa, A., Lu, L.H., Fitzgerald, D.A., Klumpp, H., Fitzgerald, K.D., Monk, C.S., and Phan, K.L. (2016). Age-related changes in amygdala-frontal connectivity during emotional face processing from childhood into young adulthood. Hum. Brain Mapp. *37*, 1684–1695.

Yan, C.G., Wang, X.D., Zuo, X.N., and Zang, Y.F. (2016). DPABI: Data Processing & Analysis for (Resting-State) Brain Imaging. Neuroinformatics *14*, 339–351.

STAR★METHODS

KEY RESOURCES TABLE

REAGENT or RESOURCE	SOURCE	IDENTIFIER
Deposited Data		
The full dataset will be made available upon request	N/A	N/A
Software and Algorithms		
MATLAB	MathWorks	https://www.mathworks.com/
SPM	Wellcome Trust Centre for Neuroimaging (UCL)	www.fil.ion.ucl.ac.uk/spm
DPABI	Yan et al., 2016	http://rfmri.org/dpabi
FSL	Smith et al., 2004	https://fsl.fmrib.ox.ac.uk/fsl/fslwiki
PANDA	Cui et al., 2013	https://www.nitrc.org/projects/panda/
DRAMMS	Ou et al., 2011	https://www.cbica.upenn.edu/sbia/software/dramms/
SPSS	IBM SPSS	http://www.spss.com.hk/software/statistics/

CONTACT FOR REAGENT AND RESOURCE SHARING

Further information and requests for resources should be directed to and will be fulfilled by the Lead Contact, Joseph W. Kable (kable@psych.upenn.edu).

EXPERIMENTAL MODEL AND SUBJECT DETAILS

Participants

Participants were recruited as part of the *Retraining Neurocognitive Mechanisms of Cancer Risk Behavior (RNMCRB)* study. For the *RNMCRB* study, participants were randomized to receive either 10 weeks of adaptive cognitive training (Lumosity games) or non-adaptive, untargeted cognitive stimulation (simple computerized video games) and underwent pre- and post-intervention brain scans. The scanning session consisted of high-resolution T1-weighted anatomical MRI, RS-fMRI, DTI, and fMRI during both risk tolerance and delay discounting tasks. The exclusion criteria for this study were: 1) history of brain injury, 2) history of psychiatric or substance disorders, 3) current use of psychotropic medication, 4) current use of chewing tobacco, snuff, or smoking cessation products, 5) left-handedness, and 6) intellectual disability (<90 score on Shipley's IQ test). As the *RNMCRB* study was designed to assess changes in decision-making in response to cognitive training, people with extreme decision preferences, at floor or ceiling on our assessments, were also excluded from participating in the study (discount rate $k < 0.0017$ or $k > 0.077$; risk tolerance $\alpha < 0.34$ or $\alpha > 1.32$; these criteria were the estimated 10^{th} and 90^{th} percentiles of the normal range in discount rate and 5^{th} and 95^{th} percentiles of the normal range in risk tolerance). A previous report has described the main trial outcomes, which found no effect of cognitive training relative to the active control on brain activity, decision-making or cognitive performance (Kable et al., 2017). All study procedures were approved by the Institutional Review Board of the University of Pennsylvania. All participants provided written informed consent.

Here we analyzed only the baseline (pre-treatment) data. Of the full cohort at baseline (n = 166), 145 had T1-weighted MRI, RS-fMRI and DTI images. Thirty-seven individuals out of 145 were excluded because of (i) low DTI quality (temporal signal to noise ratio, TSNR < 6.47 [suggested by Roalf et al., 2016]; n = 17), (ii) excessive head motion (>2.5 mm of translation or 2.5° of rotation and >0.31 mm [>2 SD from the group mean] for mean frame-wise displacement [FD; Power et al., 2012]) on RS-fMRI (n = 15); and (iii) outliers (> 3 SD from the group mean) on the degree of risk tolerance (n = 2) and node strength (n = 3). Therefore, 108 participants (64/44 males/females; age [mean ± SD], 24.36 ± 4.69 years; IQ, 111.24 ± 6.60; risk tolerance α, 0.69 ± 0.31) were used in the final analysis.

METHOD DETAILS

Risk tolerance task

Participants chose between a smaller reward available with certainty and a larger reward available with some risk for each of 120 trials. The smaller-certain reward was fixed at 100% chance of $20 and the larger-risky reward was varied from trial to trial. The

magnitude of the larger-risky reward varied from $21 to $85 and the probability of obtaining it varied from 9% to 98%. At the end of the experiment, participants received the item they chose on one randomly selected trial from the choice tasks (delay discounting and risk tolerance), in addition to visit compensation. If the trial chosen was from the risk tolerance task and the participant selected the risky option, the gamble was resolved by the roll of a die. The primary behavioral outcome was the subject's degree of risk tolerance. Risk tolerance was estimated by fitting a logistic regression that assumes a person's decisions are a stochastic function of the difference in subjective value between the two options. Participants' individual choice data were fit with the following logistic function using maximum likelihood estimation:

$$P_1 = \frac{1}{1 + \exp(-\beta(SV_1 - SV_2))},\ P_2 = 1 - P_1$$

where P_1 refers to the probability that the participant chose the risky option and P_2 refers to the probability that the participant chose the safe option. SV_1 and SV_2 refer to the participant's estimated subjective value of the risky option and the safe option respectively. β was used as a scaling factor and was fitted for each subject. For our gambles, in which there is only one reward with a given probability (p, with a $1-p$ chance of no reward), we assumed that SV (subjective values for the risky option and safe option, respectively) followed the functional form of expected utility, a power-law function of the reward amount (A) and the probability (p) of winning:

$$SV_{EU} = p \times A^{\alpha}$$

where α is the participant's degree of risk tolerance. Risk tolerance α's were log-transformed to normalize the distribution before subsequent statistical analysis. Larger values of α indicate a greater degree of risk tolerance or a lesser degree of risk sensitivity; $\alpha > 1$ (< 1) indicates risk seeking (aversion) and $\alpha = 1$ indicates risk neutrality (i.e., participants choose according to expected value).

To confirm that our findings were robust to the specification of risk tolerance, we also conducted sensitivity analyses using several alternative measures of risk attitudes. We fit two alternative models of subjective value based on the risk-return or mean-variance frameworks. In the classic formulation of risk-return models, SV is a function of the expected value (EV) and variance (Var) of the gamble, given a risk aversion parameter b.

$$SV_{RR} = EV - b_{RR} \times Var$$

$$EV = p \times A$$

$$Var = p \times (A - EV)^2 + (1 - p) \times (A - 0)^2$$

An alternative formulation uses the coefficient of variation (CV) rather than the variance (Weber et al., 2004).

$$SV_{RRW} = EV - b_{RRW} \times CV$$

$$CV = \frac{\sqrt{Var}}{EV}$$

In both of these cases, b measures a person's aversion to risk, with higher values indicating more risk aversion and less risk tolerance. We also used the percentage of risky choices, both over all choices (n = 120) and in probability tertiles (0% < p $\leq$ 33%, n = 25; 33% < p $\leq$ 66%, n = 64; 66% < p, n = 31), as a model-free measure of risk tolerance.

Image acquisition

All MRI data were acquired using a Siemens 3T Trio scanner (Siemens, Erlangen, Germany). T1-weighted images were obtained with a magnetization-prepared rapid gradient echo (MPRAGE) sequence [repetition time (TR)/echo time (TE) = 1630/3.11 ms, voxel size = 0.94 × 0.94 × 1.0 mm^3, 160 axial slices]. RS-fMRI data were collected using an echo planar imaging (EPI) sequence (TR/TE = 3000/25 ms; voxel size = 3 × 3 × 3 mm^3; 53 interleaved axial slices with no gaps; 160 volumes during 8 min and 6 s). During RS-fMRI scanning, participants were asked to keep their eyes open and maintain fixation. DTI data were acquired using a single-shot spin echo EPI sequence (TR/TE = 8000/82 ms, voxel size = 1.88 × 1.88 × 2 mm^3, 70 interleaved slices, GRAPPA factor = 3, 30 diffusion directions with b-values of 1000 s/mm^2 and 1 image with b = 0 s/mm^2).

QUANTIFICATION AND STATISTICAL ANALYSIS

RS-fMRI analysis

RS-fMRI data were preprocessed using the Data Processing & Analysis for (Resting-State) Brain Imaging toolbox in MATLAB (DPABI; Yan et al., 2016) and SPM8 (http://www.fil.ion.ucl.ac.uk/spm). After discarding the first 4 scans, slice-timing correction, motion

realignment, nuisance signal correction, and spatial normalization to the MNI template were performed. For nuisance signal correction, the following nuisance parameters were included as regressors within the general linear model; 6 motion parameters and their first derivatives, 5 principal components extracted from a combined white matter (WM)/ cerebrospinal fluid (CSF) mask using the CompCor method (Behzadi et al., 2007), and a linear trend term. Next, spatial smoothing (FWMH kernel: 6 mm) and temporal band-pass filtering (0.01–0.1 Hz) were performed.

We used the 90-parcel AAL template (Tzourio-Mazoyer et al., 2002) to examine RSFC, as this template provides adequate coverage of both cortical and subcortical regions, including the amygdala. The mean time courses in each AAL parcel (as a node) were extracted, correlated with each other (using Pearson's correlation coefficients as edges), and converted to z-scores using Fisher's r-to-z transformation, in order to generate a 90 × 90 connectivity matrix per subject. These connectivity matrices were used to calculate node strength. Node strength is a measure that quantifies the importance/centrality of a node through the strength of its connections to all other nodes in a network (Rubinov and Sporns, 2010). We calculated node strength by summing the absolute values of all weighted edges (i.e., correlation coefficients) for a given node to quantify the total connectivity of a node. To define the nodes associated with individuals' risk tolerance, we performed partial correlations (covariates: age, sex, IQ, and motion indexed by mean FD) between node strength and risk tolerance. To address multiple comparisons in this analysis, we calculated a false-positive adjusted threshold ($p < 1/90 = 0.011$, where 90 is the total number of nodes) that has been used in many previous studies that compare local network measures estimated from graph-theoretical analysis (Lynall et al., 2010; Cocchi et al., 2012).

To examine the connectivity of significant nodes (i.e., amygdala per hemisphere; Figure 2A), we generated seed-to-voxel FC maps. To determine the regions showing an association between these seed FC maps (seeded by each amygdala) and risk tolerance, we performed multiple regression analysis at the voxel level, while controlling for age, sex, IQ, and mean FD. The results were corrected for multiple comparisons to a significance level of $p < 0.05$ (height threshold of $p < 0.001$, uncorrected, combined with extent threshold of $p < 0.05$) by the AlphaSim program as implemented in the DPABI software (DPABI_V2.3_170105). We note that the bug reported by Eklund et al. (2016) had been fixed in the software version used in this study (see http://rfmri.org/dpabi).

DTI analysis

DTI data were preprocessed using the Pipeline for Analyzing braiN Diffusion imAges toolbox in MATLAB (PANDA; Cui et al., 2013), which uses processing functions of established packages, such as FSL (http://fsl.fmrib.ox.ac.uk/fsl/fslwiki/) and the Diffusion Toolkit (https://www.nitrc.org/projects/trackvis/). Briefly, a brain mask was estimated using b0 images. Diffusion images were registered to the b0 image using an affine transformation to correct the eddy current-induced distortions and simple head-motion. Fiber tracts were estimated using bedpostX (Behrens et al., 2003) with two crossing fibers per voxel. Then, probabilistic tractography analysis was performed to assess structural connectivity from seed to target using probtrackX (Behrens et al., 2007) in FSL with default options (5000 streams per each voxel seed, 0.5 mm step lengths, curvature thresholds = 0.2). The target masks were defined by RS-fMRI analysis (i.e., the clusters showing significant correlations between risk tolerance and RSFC to each amygdala) at a height threshold of $p < 0.005$, uncorrected, combined with an extent threshold at a corrected $p < 0.05$. To define and measure the integrity of the structural tract from DTI, we used a slightly lower cluster-forming threshold because tractography analysis is less reliable with very small clusters. The target and seed masks were transformed from MNI space to each subject's native space, where probtrackX was ran. This tractography analysis identifies the most likely pathway between each seed voxel and each target voxel by calculating the probability of connectivity between them; that is, the values in voxels on resulting images represent the number of sampled streamlines that successfully reached the target region. We normalized values in voxels by dividing by the total number of sampled streamlines and thresholded at 10% to exclude spurious connections. Note that we observed similar results under a wide range of thresholds, from 2% to 30%. We then took a mean value for all voxels within the defined tract, which is widely used as a measure of tract strength between two brain regions (Johansen-Berg and Rushworth, 2009; Croxson et al., 2005). Because the tract strength values were non-normally distributed, they were log-transformed before subsequent statistical analysis. We performed partial correlation (covariates: age, sex, and IQ) between risk tolerance and tract strengths.

Some previous studies have used FA values, rather than tract strengths, to investigate the link between white matter tracts and behavior (Clewett et al., 2014; Kim et al., 2016; Leong et al., 2016). Thus, we also performed partial correlation (covariates: age, sex, and IQ) between FA values extracted from each tract and tract strengths and risk tolerance. This exploratory analysis showed that the tract strength in the right amygdala–mPFC tract that showed a significant association with risk tolerance also had a significant positive correlation with its FA value ($r = 0.386$, $p < 0.001$), though the FA value itself had no association with risk tolerance ($r = 0.003$, $p < 0.978$; not shown).

T1-MRI analysis

T1 data were segmented into GM, WM, and CSF tissue maps in native space using SPM8. Each individual's three tissue maps were combined into a single volume and the combined volume was registered to a single MNI-space template using the DRAMMS deformable registration package (Ou et al., 2011; https://www.cbica.upenn.edu/sbia/software/dramms/). Deformation field calculated from this spatial registration was then applied to segmented images in order to generate mass-preserved volumetric maps, named Regional Analysis of Volumes Examined in Normalized Space (RAVENS) maps (Davatzikos et al., 2001). In RAVENS maps, the tissue density reflects the amount of tissue present in each participant's image at a given location, after mapping to the common template

space. The GM RAVENS maps were smoothed with 6-mm FWMH kernel. We performed partial correlation (covariates: age, sex, IQ, and total intracranial volume [TIV]) between risk tolerance and GMV of amygdala extracted from RAVENS map.

For the exploratory whole-brain VBM analysis, we conducted multiple regression on the smoothed GM RAVENS image with risk tolerance as a covariate of interest and age, sex, IQ and TIV as covariates of no interest. To correct for multiple comparisons, we applied a height threshold of $p < 0.001$ (uncorrected) and a cluster extent threshold of $p < 0.05$ using AlphaSim (Figure S1, Related to Figure 5).

Given previous reports of a positive relationship between risk tolerance and rPPC GMV (Gilaie-Dotan et al., 2014; Grubb et al., 2016), we also conducted an exploratory ROI analysis with an rPPC ROI defined independently based on Gilaie-Dotan et al. (2014), using the mask at https://yale.app.box.com/v/levylab-gilaie-dotan-etal-2014.

Linear regression analysis to estimate brain predictors of risk tolerance

We performed linear regression analyses to examine the ability of brain variables to predict an individual's risk tolerance using SPSS. Before statistical analysis, the amygdala GMV extracted from RAVENS map was divided by TIV and the effects of age, sex, and IQ were regressed out of all brain variables. Then, a linear regression analysis with each brain variable alone and with all brain variables together (node strength, RSFC extracted from seed-based FC result, GMV, and tract strength of amygdala) was performed separately for each hemisphere.

DATA AND SOFTWARE AVAILABILITY

The full dataset will be made available upon request.

Neuron, Volume *98*

Supplemental Information

Amygdala Functional and Structural Connectivity Predicts Individual Risk Tolerance

Wi Hoon Jung, Sangil Lee, Caryn Lerman, and Joseph W. Kable

Supplemental Data
Figure S1. Related to Figure 5.

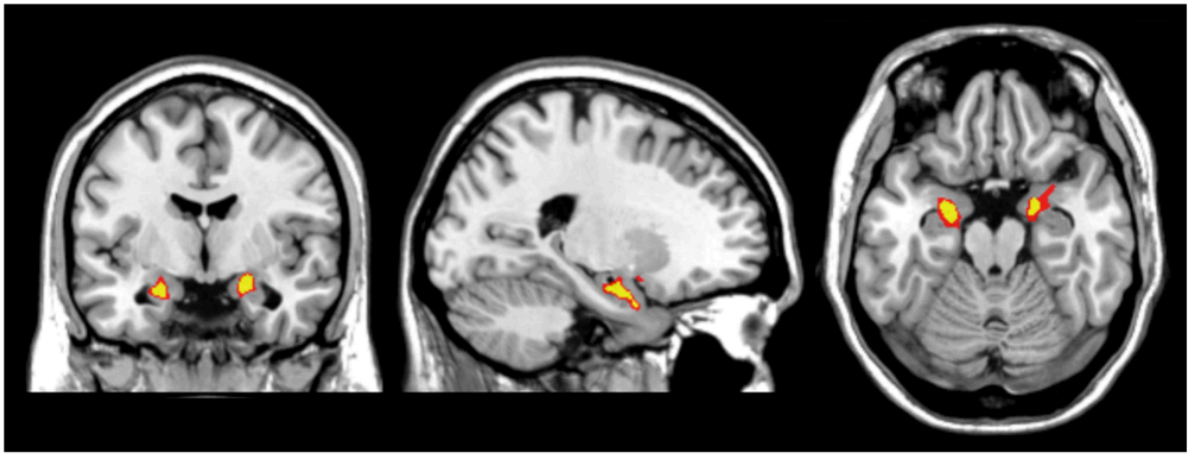

Figure S1. Regions showing association between risk tolerance and gray matter volume (GMV) at whole-brain voxel level. Risk tolerance had higher association with GMV in bilateral amygdalae than GMV in any other regions (yellow, a height threshold of $p<0.001$, uncorrected; red, a height threshold of $p<0.005$, uncorrected; all clusters survive correction for multiple comparisons using an extent threshold of $p<0.05$).